10.24425/acs.2022.140868

Archives of Control Sciences
Volume 32(LXVIII), 2022
No. 1*, pages 123–152*

A new multistable jerk chaotic system, its bifurcation analysis, backstepping control-based synchronization design and circuit simulation

Sundarapandian VAIDYANATHAN, Khaled BENKOUIDER and Aceng SAMBAS

In this work, we present results for a new dissipative jerk chaotic system with three quadratic terms in its dynamics. We describe the bifurcation analysis for the new jerk system and also show that the proposed system exhibits multi-stability. Next, we describe a backstepping control-based synchronization design for a pair of new jerk chaotic systems. MATLAB simulations are put forth to exhibit the various findings in this work. Furthermore, we exhibit a circuit simulation for the new jerk system using MultiSim.

Key words: chaos, jerk systems, bifurcation, multistability, attractors, backstepping control and circuit design

1. Introduction

Chaotic dynamical systems are useful in several domains such as [1,2], neural networks [3–5], robotics [6,7], power systems [8,9], circuits [10,11], memristors [12–14], oscillations [15,16], communications [17,18], etc.

Jerk differential equations arise in mechanical systems featuring the third derivative (*jerk*) of the displacement of a moving particle. Jerk differential equations can be enlisted as follows:

$$\frac{d^3y}{dt^3} + G\left(y, \frac{dy}{dt}, \frac{d^2y}{dt^2}\right) = 0. \tag{1}$$

S. Vaidyanathan (corresponding author, e-mail: sundarvtu@gmail.com) is with School of Electrical and Computing, Vel Tech University, 400 Feet Outer Ring Road, Avadi, Chennai-600092, Tamil Nadu, India.

K. Benkouider (e-mail: benkouider.khaled@gmail.com) is with Non Destructive Testing Laboratory, Automatic Department, Jijel University, BP 98, 18000, Jijel, Algeria.

A. Sambas (e-mail: acengs@umtas.ac.id) is with Department of Mechanical Engineering, Universitas Muhammadiyah Tasikmalaya, Tasikmalaya 46196, West Java, Indonesia.

Received 13.07.2021.

Using phase variables, the jerk DE (1) can be put in a system form as

$$\begin{aligned} \dot{y}_1 &= y_2\,, \\ \dot{y}_2 &= y_3\,, \\ \dot{y}_3 &= -G\left(y_1, y_2, y_3\right). \end{aligned} \tag{2}$$

Applications of jerk systems in chaos theory have been studied in the control literature [19–24]. Sambas *et al.* [19] proposed a jerk model which is endowed with chaos, multistability and saddle-foci equilibrium points. Li *et al.* [20] proposed a memristic jerk circuit with hidden chaotic oscillation. Braun and Mereu [21] found zero-Hopf bifurcation in a chaotic jerk system. Kengne *et al.* [22] proposed image encryption design using a quintic jerk circuit. Xu *et al.* proposed an assymetric diode-bridge-based jerk circuit with multistability. Lamamra *et al.* proposed a chaotic jerk system and described circuit simulation and backstepping synchronization.

In this work, we put forth our results of a new jerk system exhibiting dissipative chaos and multistability. We carry out an extensive bifurcation analysis on the new jerk system and detail the results obtained. We also present control results for the new jerk system by devising backstepping control based synchronization design. Circuit simulation for the new jerk system is presented at the end of this work, which aids in practical implementation of the jerk system.

2. A new jerk system with three quadratic nonlinear terms

In this work, we propose a new jerk system modelling by the jerk dynamics

$$\begin{aligned} \dot{y}_1 &= y_2\,, \\ \dot{y}_2 &= y_3\,, \\ \dot{y}_3 &= -ay_1 - by_2 - y_3 - y_1y_2 - cy_1^2 + y_2^2\,. \end{aligned} \tag{3}$$

We designate the state of the jerk system (3) by $Y = (y_1, y_2, y_3)$.

It shall be established in this work via Lyapunov exponents that the system (3) exhibits a chaotic attractor when the parameters undertake the values

$$a = 2, \qquad b = 0.1, \qquad c = 0.2. \tag{4}$$

When $Y(0) = (0.4, 0.2, 0.4)$ and the parameters are as in (4), the Lyapunov exponents of the jerk system (3) were evaluated for $T = 1E5$ seconds as

$$\psi_1 = 0.1525, \quad \psi_2 = 0, \quad \psi_3 = -1.1525. \tag{5}$$

This leads us to the deduction that the jerk system (4) has dissipative chaotic motion for $(a, b, c) = (2, 0.1, 0.2)$. Figure 1 displays the signal plots of the 3-D jerk system (3) for $Y(0) = (0.4, 0.2, 0.4)$ and $(a, b, c) = (2, 0.1, 0.2)$.

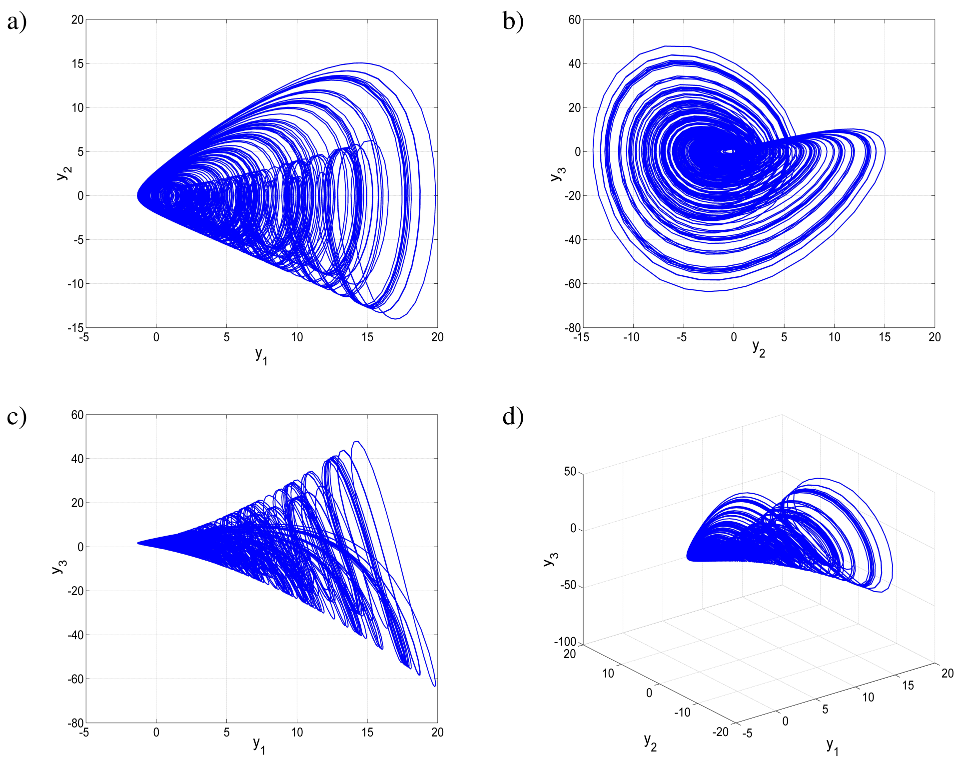

Figure 1: MATLAB signal plots of the jerk system (3) for $Y(0) = (0.4, 0.2, 0.4$ and $(a, b, c) = (2, 0.2, 0.2)$: a) (y_1, y_2)-plane, b) (y_2, y_3)-plane, c) (y_1, y_3)-plane, d) the 3-D space

The balance points of the system (3) are calculated by solving the equations

$$y_2 = 0, \tag{6a}$$
$$y_3 = 0, \tag{6b}$$
$$-ay_1 - by_2 - y_3 - y_1y_2 - cy_1^2 + y_2^2 = 0. \tag{6c}$$

It is easy to show that there are two balance points for the jerk system (3) given by $B_0 = (0, 0, 0)$ and $B_1 = (-a/c, 0, 0)$.

For the chaotic case $(a, b, c) = (2, 0.1, 0.2)$, the balance points are found as $B_0 = (0, 0, 0)$ and $B_1 = (-10, 0, 0)$.

Using Lyapunov stability theory by the first method, it can be easily established that B_0 is a saddle-focus, while B_1 is a saddle point.

The new jerk system (3) exhibits multistability as it possesses two coexisting chaotic attractors for $(a, b, c) = (2, 0.1, 0.2)$ but two different phases $Y_0 = (0.4, 0.2, 0.4)$ (blue orbit) and $Z_0 = (-0.8, 0.4, -0.8)$ (red orbit).

Figure 2 shows that the jerk system (3) has coexistence of two chaotic attractors for $(a, b, c) = (2, 0.1, 0.2)$, where the blue attractor corresponds to the initial state $Y_0 = (0.4, 0.2, 0.4)$ and the red attractor corresponds to the initial state $Z_0 = (-0.8, 0.8, -0.8)$.

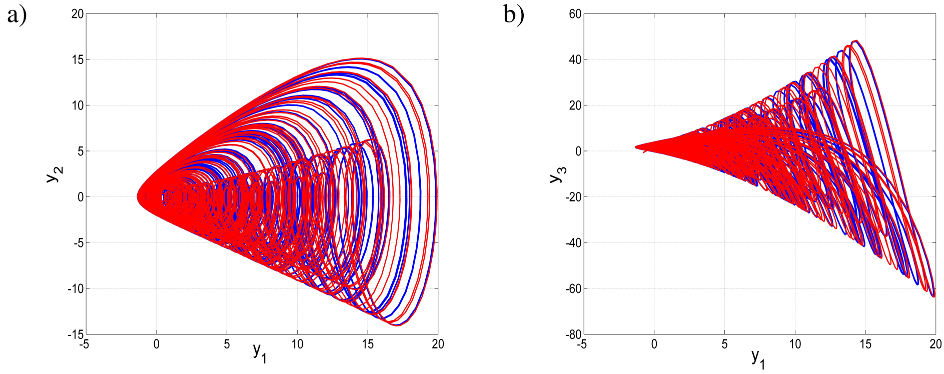

Figure 2: Multistability of the jerk system (3): Two coexisting chaotic attractors for $(a, b, c) = (2, 0.1, 0.2)$ and two initial phases $Y_0 = (0.4, 0.2, 0.4)$ (blue orbit) and $Z_0 = (-0.8, 0.8, -0.8)$ (red orbit): a) (y_1, y_2) plane and b) (y_1, y_3) plane

3. Bifurcation analysis and multistability of the new jerk system

Nonlinear systems can have different dynamical behaviors according to the values of their parameters. There may be ranges of parameters for which the system moves from one qualitative dynamical behavior to another. This qualitative change of behaviors is known as a bifurcation and it is obtained either through the bifurcation diagram or through the Lyapunov exponents spectrum. As it is known, the Lyapunov exponent is a measure of exponential rates of convergence and divergence for an uncertainty on the trajectories initial points. When it is positive the uncertainty increases, which means divergence of trajectories and appearance of chaos. Therefore, Lyapunov exponents spectrum and bifurcation diagram represent the two most important tools to analyse the dynamical behaviour of a system. In this section, dynamical behaviours and complexity of the new jerk system (3) are investigated by using numerical calculations with the positive parameters a, b and c varying.

3.1. Parameter a varying

To investigate the sensitivity of the jerk system (3) to the variation of parameter a, we fix $b = 0.1$, $c = 0.2$ and vary a between 0.2 and 2.

Lyapunov exponents spectrum and the corresponding bifurcation diagram of the jerk system (3) when a belongs to the set of values $[0.2, 2]$ and for the initial state $Y(0) = (0.4, 0.2, 0.4)$ are depicted in Figure 3.

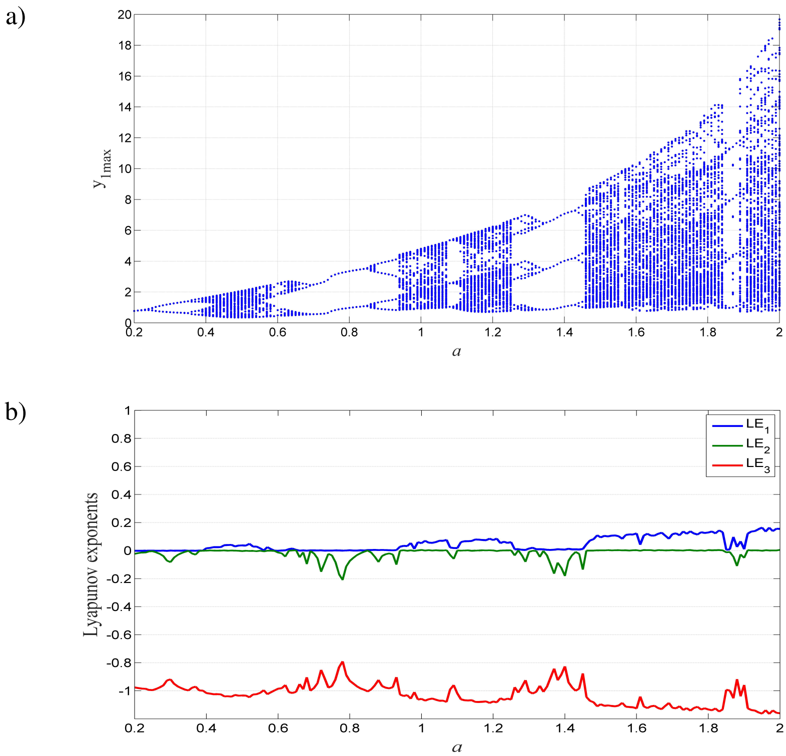

Figure 3: Dynamic analysis of the new jerk system (3) with parameter a varying and $b = 0.1$, $c = 0.2$: a) Bifurcation diagram and b) Lyapunov exponents spectrum

From Figure 3, we can see a good agreement between the bifurcation diagram and the Lyapunov exponents spectrum. Figure 3 shows that the proposed jerk system (3) can exhibit periodic behaviour with no positive Lyapunov exponents indicating no complexity of the dynamics when:

$$a \in \big([0.10,\ 0.40],\ [0.61,\ 0.94],\ [1.26,\ 1.45]\big). \tag{7}$$

Also, the new jerk system (3) can involve into a chaotic attractor with one positive Lyapunov exponents when:

$$a \in \big([0.41,\ 0.60],\ [0.95,\ 1.25],\ [1.46,\ 2]\big). \tag{8}$$

There is also a tiny window of periodic behaviour sandwiched in chaotic bands when:

$$a \in \big([1.85,\ 1.88]\big). \tag{9}$$

Different dynamical behaviors of the jerk system (3) for special values of parameter a are shown in Figure 4.

a)

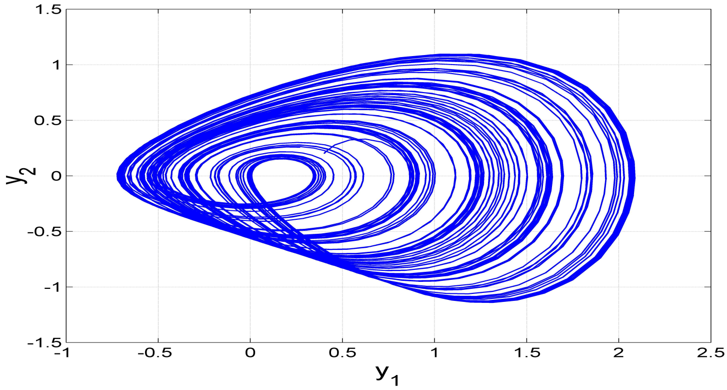

$a = 0.5$

b)

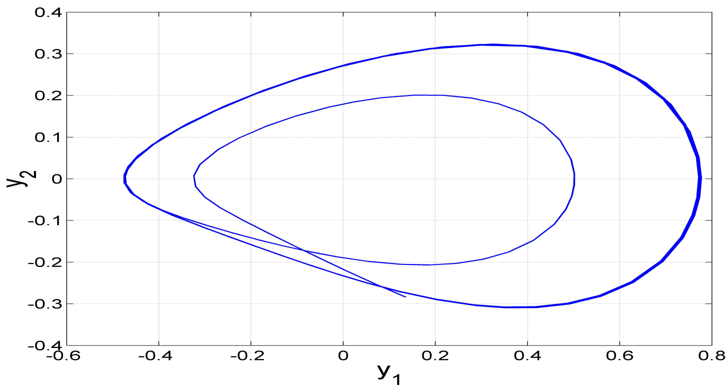

$a = 0.3$

Figure 4: Phase portraits of the new jerk system (3) for two different values of a: a) (y_1, y_2) chaotic attractor and b) (y_1, y_2) periodic attractor

In addition, it is clear from the bifurcation diagram of Figure 3 that the jerk system (3) experiences the well-known period-doubling route to chaos and the interesting scenario of the antimonotonicity.

3.1.1. Period-doubling description

As depicted in the bifurcation diagram of Figure 3, the system experiences period-doubling cascade for increasing values of the parameter a. Therefore, we can observe the well-known period-doubling route to chaos (period-1 $\longrightarrow$ period-2 $\longrightarrow$ period-4 $\longrightarrow$ period-8 $\longrightarrow$ chaos) for specified values of parameter a as shown in Figure 5.

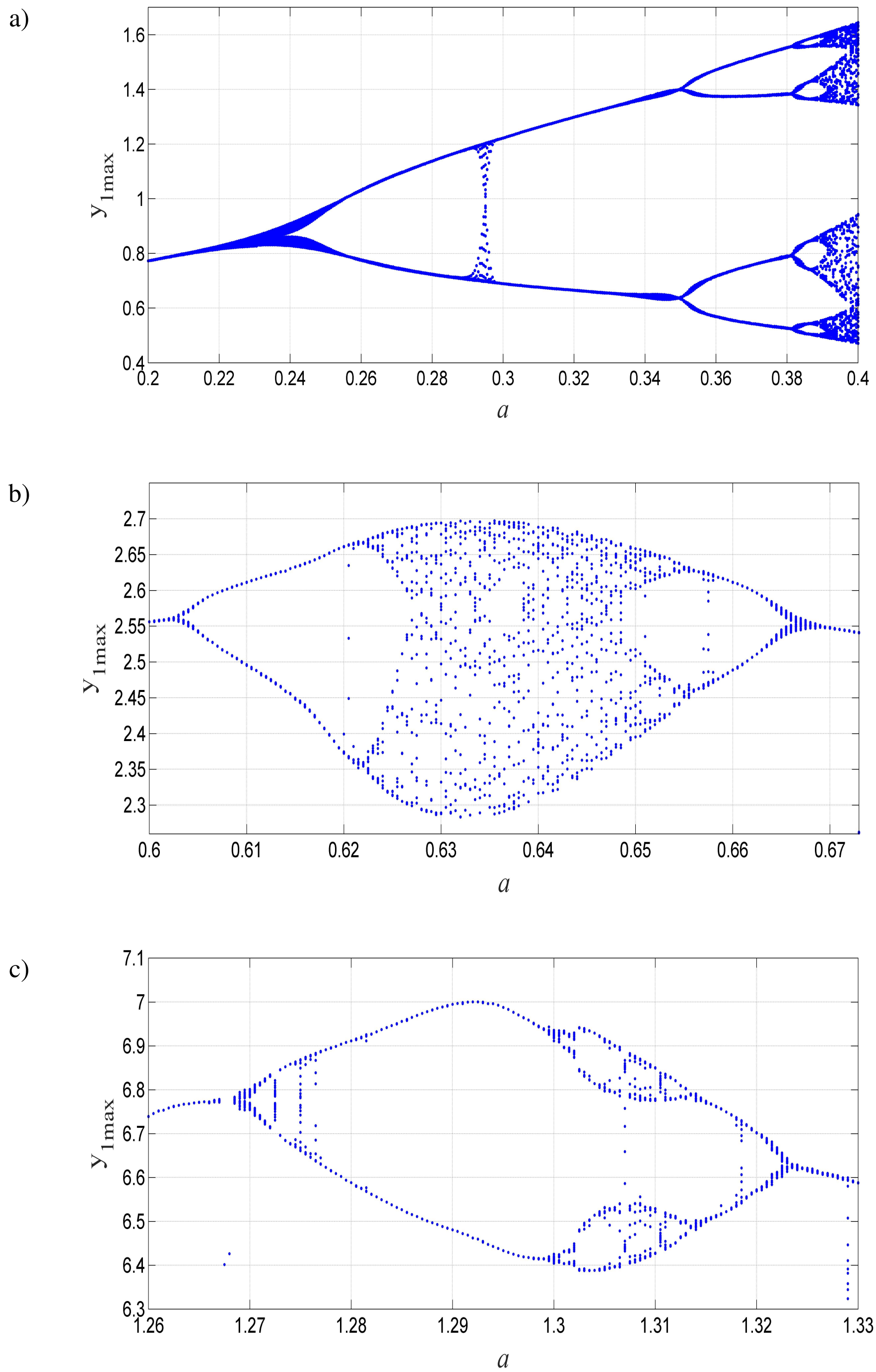

Figure 5: Three independents period doubling cascade route to chaos in the jerk system (3) when parameter a varies: a) $a \in [0.2, 0.4]$, b) $a \in [0.7, 0.95]$ and c) $a \in [1.36, 1.46]$

When $a \in [0.20, 0.24]$, the jerk system (3) has period-1 attractor.

When $a \in [0.25, 0.35]$, the jerk system (3) has period-2 attractor.

When $a \in [0.360, 0.382]$, the jerk system (3) has period-4 attractor.

When $a \in [0.383, 0.4]$, the jerk system (3) has period-8 attractor.

When $a \in [0.4, 0.6]$, the jerk system (3) has chaotic attractor which makes an end for the first period-doubling cascade.

When $a \in [0.70, 0.85]$, the jerk system (3) has period-1 attractor.

When $a \in [0.86, 0.94]$, the jerk system (3) has period-2 attractor.

When $a \in [0.95, 1.25]$, the jerk system (3) has chaotic attractor which makes an end for the second period-doubling cascade.

When $a \in [1.36, 1.43]$, the jerk system (3) has period-1 attractor.

When $a \in ([1.44, 1.45])$, the jerk system (3) has period-2 attractor.

When $a \in [1.46, 2]$, the jerk system (3) has chaotic attractor which makes an end for the last period-doubling cascade produced by the jerk system (3) when the parameter a varies.

The various attractors (numerical simulations) illustrating the above described routes to chaos are listed in Table 1 and plotted in Figures 6, 7 and 8.

Table 1: Dynamics, bifurcation diagrams and attractors of the new jerk system (3) with parameter a varying

a range	a value	Dynamics	Bifurcation Diagram	Attractor
$[0.20, 0.24]$	0.2	Period-1	Figure 3a	Figure 6a
$[0.25, 0.35]$	0.32	Period-2	Figure 3a	Figure 6b
$[0.36, 0.382]$	0.37	Period-4	Figure 3a	Figure 6c
$[0.383, 0.40]$	0.386	Period-8	Figure 3a	Figure 6d
$[0.41, 0.60]$	0.5	**Chaos**	Figure 3a	Figure 6e
$[0.61, 0.69]$	0.65	Full Feigenbaum remerging tree	Figure 9a	Figure 9c
$[0.70, 0.85]$	0.75	Period-1	Figure 3a	Figure 7a
$[0.86, 0.93]$	0.9	Period-2	Figure 3a	Figure 7b
$[0.94, 1.25]$	1.2	**Chaos**	Figure 3a	Figure 7c
$[1.26, 1.35]$	1.3	Period-4 bubble	Figure 9b	Figure 9d
$[1.36, 1.43]$	1.4	Period-1	Figure 3a	Figure 8a
$[1.44, 1.45]$	1.45	Period-2	Figure 3a	Figure 8b
$[1.46, 2]$	1.7	**Chaos**	Figure 3a	Figure 8c

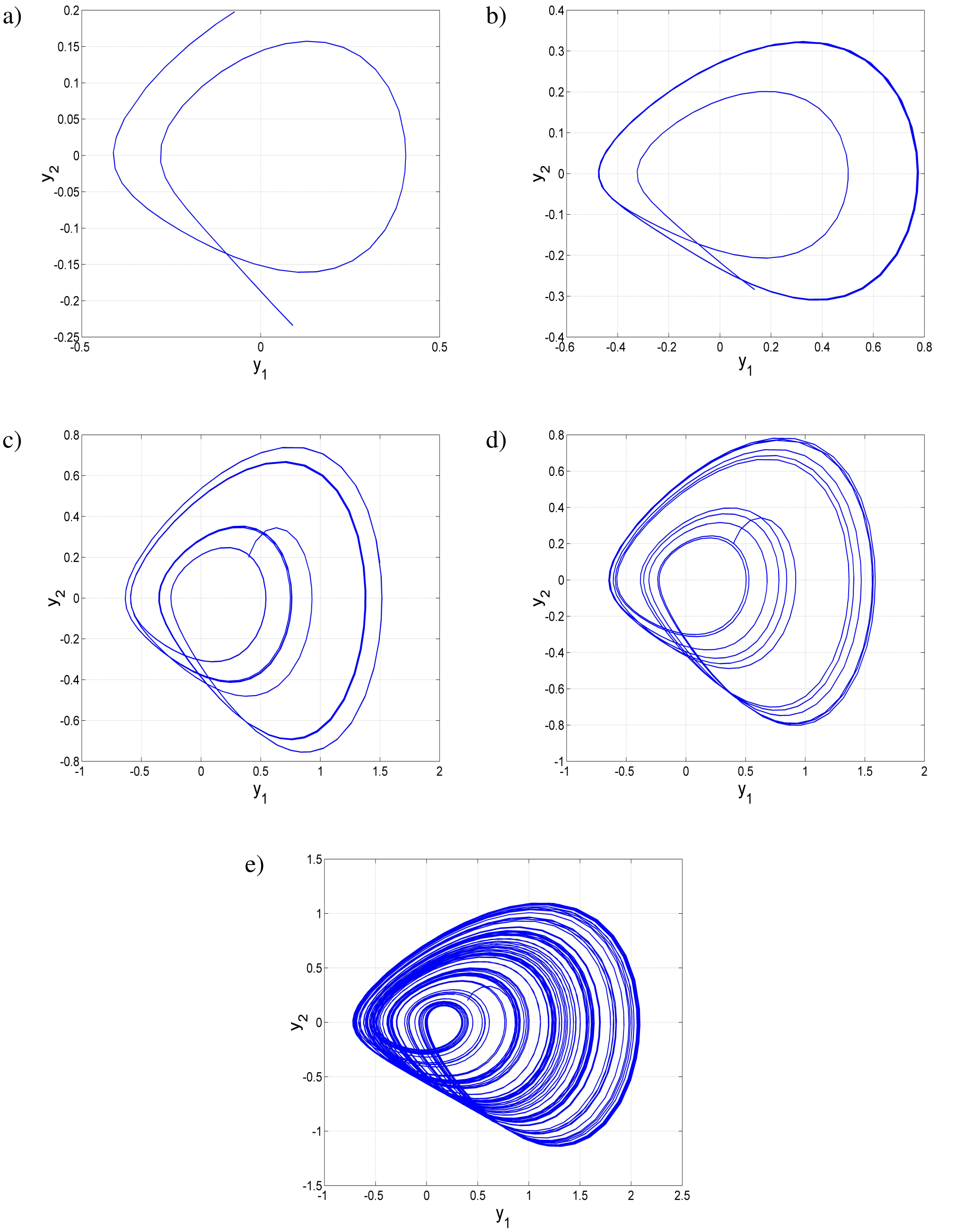

Figure 6: Numerical phase space trajectories showing the first classical period doubling route to chaos in the jerk system (3) when parameter a varies: (a) Period-1 for $a = 0.2$, (b) Period-2 for $a = 0.32$, (c) Period-4 for $a = 0.37$, (d) Period-8 for $a = 0.386$, (e) chaos for $a = 0.5$

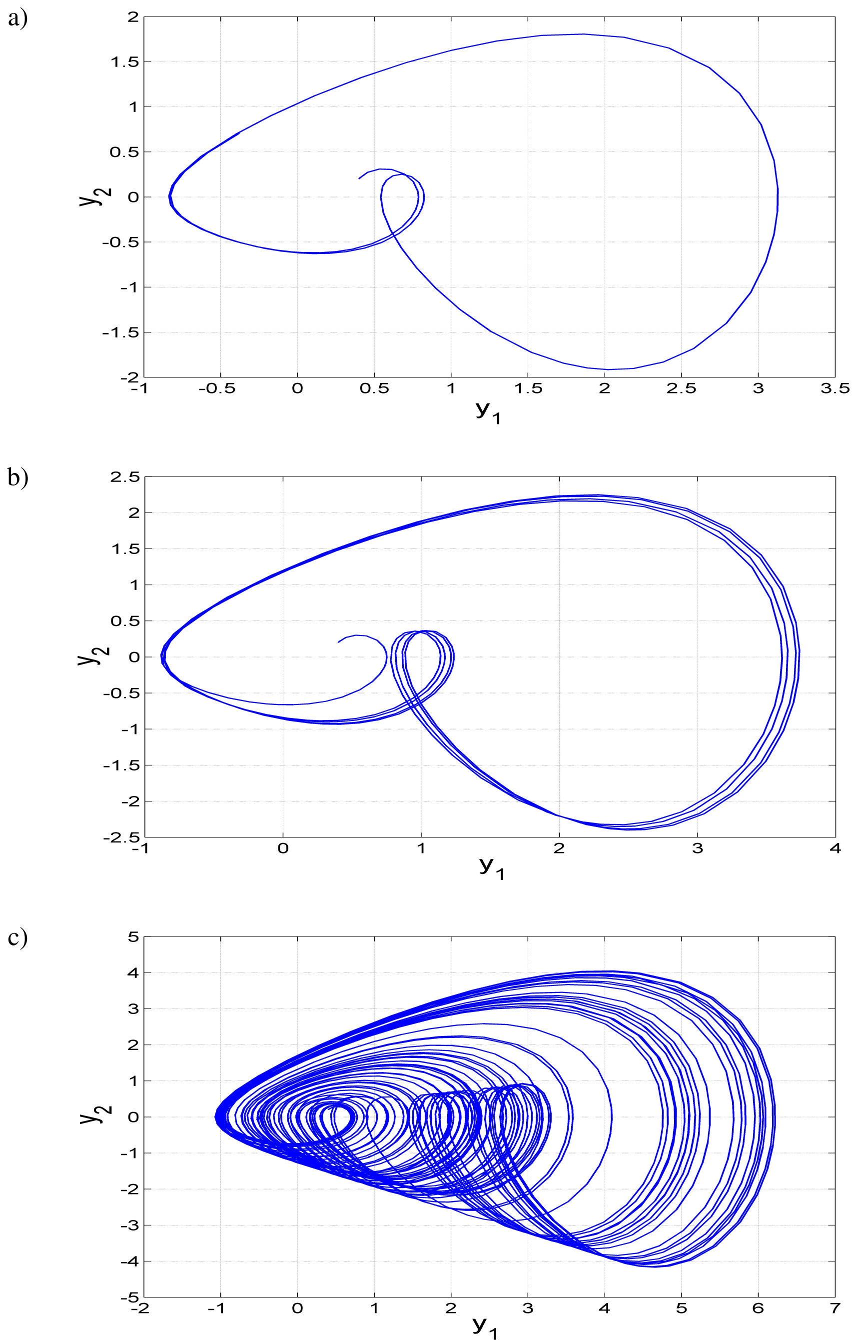

Figure 7: Numerical phase space trajectories showing the second classical period doubling route to chaos in the jerk system (3) when parameter a varies: a) Period-1 for $a = 0.75$, b) Period-2 for $a = 0.9$, c) chaos for $a = 1.2$

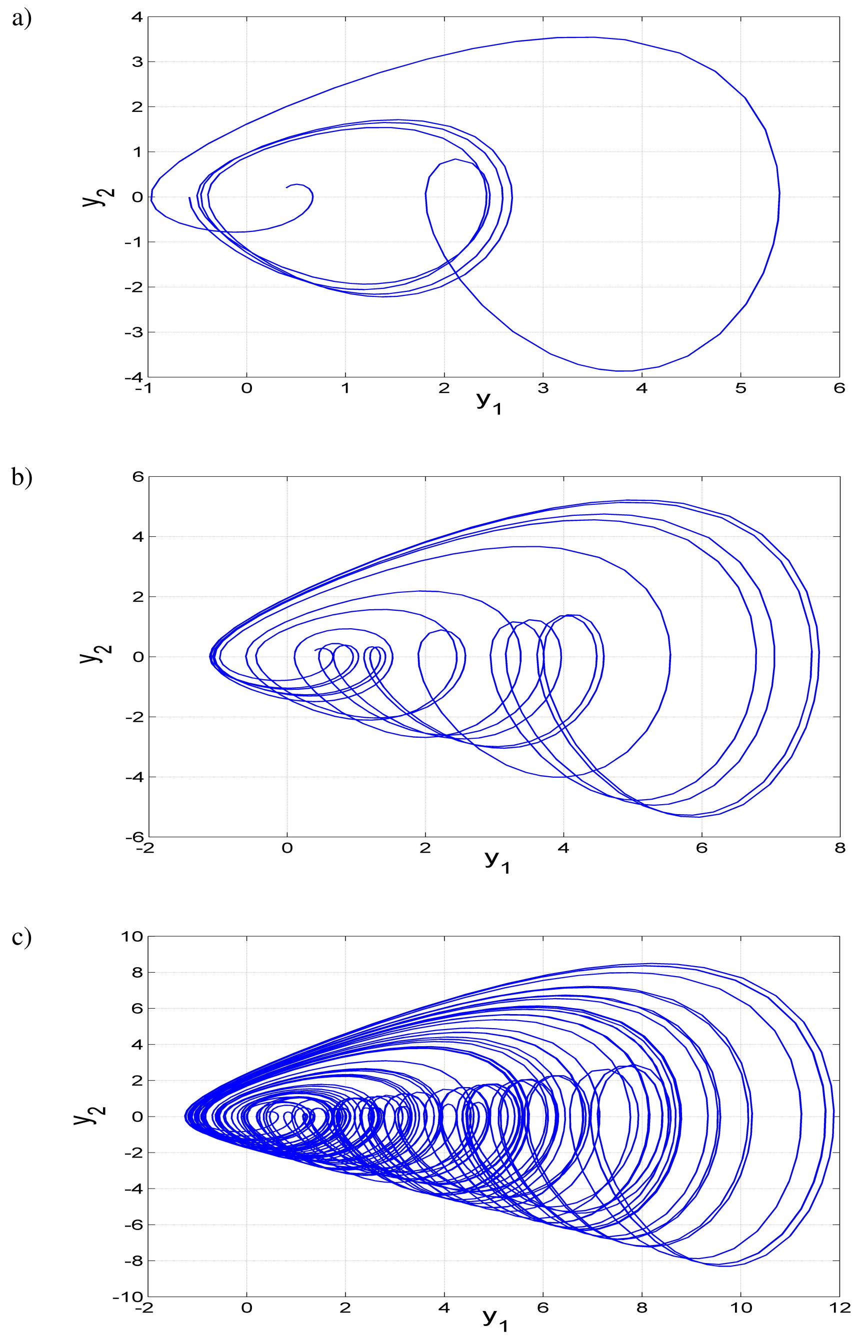

Figure 8: Numerical phase space trajectories showing the third classical period doubling route to chaos in the jerk system (3) when parameter a varies: a) Period-1 for $a = 1.4$, b) Period-2 for $a = 1.45$, c) chaos for $a = 1.7$

3.1.2. Antimonotonicity

As the route to chaos is the classical period doubling bifurcation, it is obvious that the jerk system (3) experiences the antimonotonicity. This phenomenon is described by the creation of periodic orbits followed by their destruction via a reverse period-doubling scenario as a bifurcation parameter is varied. It is easily be noticed that in Figure 9(a) which is derived from the bifurcation diagram of Figure 3. When $a \in [1.26, 1.35]$, period-4 bubble is obtained, while, a full Feigenbaum remerging tree is observed in Figure 9(b) when $a \in [0.6, 0.7]$.

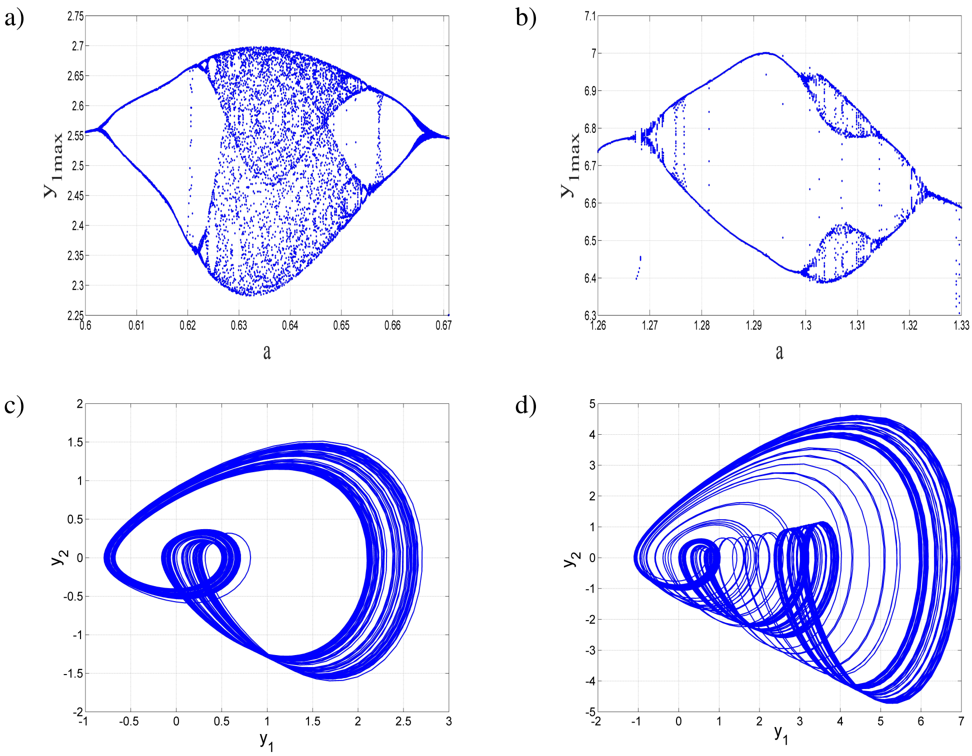

Figure 9: Bifurcation diagrams of the jerk system (3) and their corresponding attractors showing a) Full Feigenbaum remerging tree when $a \in [0.60, 0.69]$, b) Period-4 bubble when $a \in [1.26, 1.35]$, c) $y_1 - y_2$ attractor when $a = 0.65$ and d) $y_1 - y_2$ attractor when $a = 1.3$

4. Parameter b varying

To investigate the sensitivity of the jerk system (3) to the variation of the parameter b values, we fix $a = 2$, $c = 0.2$ and vary b between 0.1 and 2.

Lyapunov exponents spectrum and the corresponding bifurcation diagram of the jerk system (3) when $b \in [0.1, 2]$ and for the initial state $Y(0) = (0.4, 0.2, 0.4)$ are depicted in Figure 10 where we can see a good agreement between the bifurcation diagram and the Lyapunov exponents spectrum.

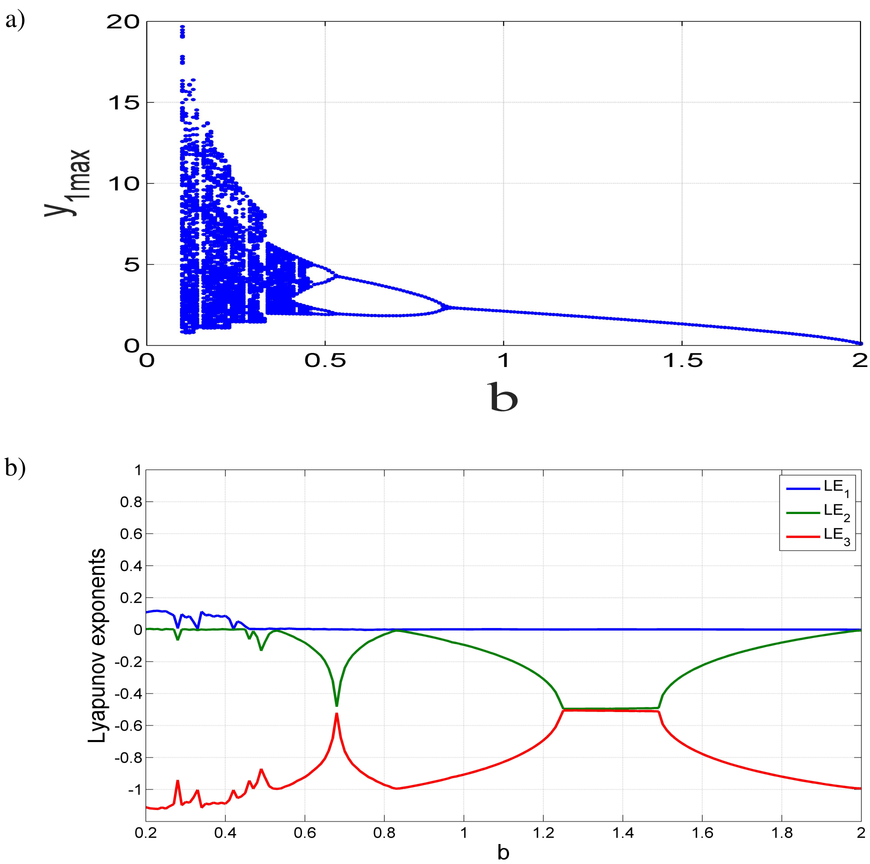

Figure 10: Dynamic analysis of the new jerk system (3) with parameter b varying and $a = 2$, $c = 0.2$: a) Bifurcation diagram and b) Lyapunov exponents spectrum

Figure 10 shows that the proposed jerk system (3) can exhibit chaotic behaviour with one positive Lyapunov exponent when $b \in [0.10, 0.44]$. Also, the new jerk system (3) can exhibit periodic behaviour with no positive Lyapunov exponent when $b \in [0.45, 2]$, which indicates no complexity of the dynamics.

There is also a tiny window of periodic behaviour sandwiched in chaotic bands when $b \in [0.32, 0.34]$.

Different dynamical behaviour of the jerk system (3) for special values of parameter b are shown in Figure 11.

a)

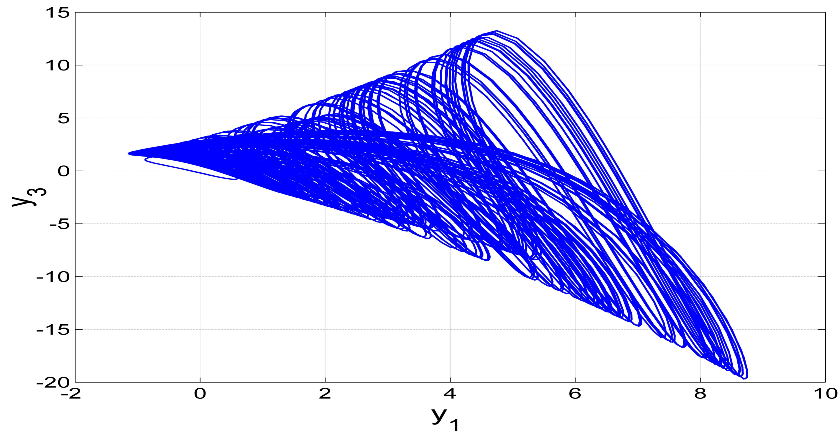

$b = 0.3$

a)

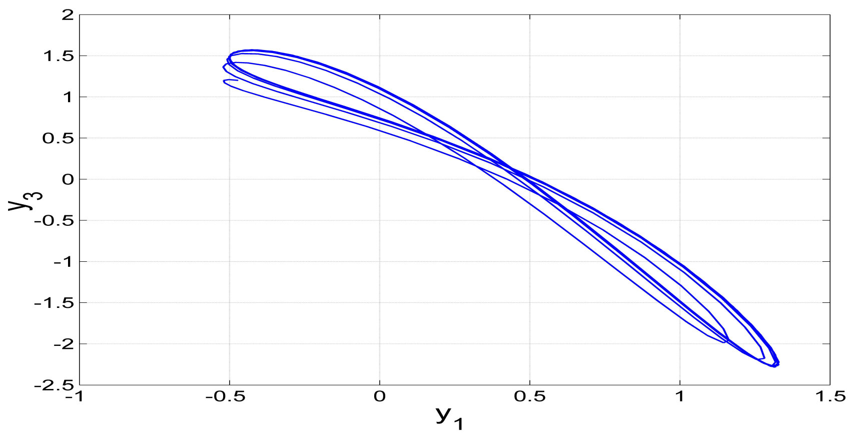

$b = 1.5$

Figure 11: Phase portraits of the new jerk system (3) for two different values of b in the (y_1, y_3) plane: a) Chaotic attractor for $b = 0.3$ and b) Periodic attractor for $b = 1.5$

In addition, it is clear from the bifurcation diagram of Figure 10 that the jerk system (3) experiences the well-known reversal period-doubling route.

4.1. Reverse period-doubling description

As depicted in the bifurcation diagram of Figure 10, the system (3) experiences period-doubling cascade for increasing values of the parameter b.

Therefore, we can observe the well know period-doubling exiting from chaos (chaos $\longrightarrow$ period-8 $\longrightarrow$ period-4 $\longrightarrow$ period-2 $\longrightarrow$ period-1) for specified values of parameter b as shown in Figure 12.

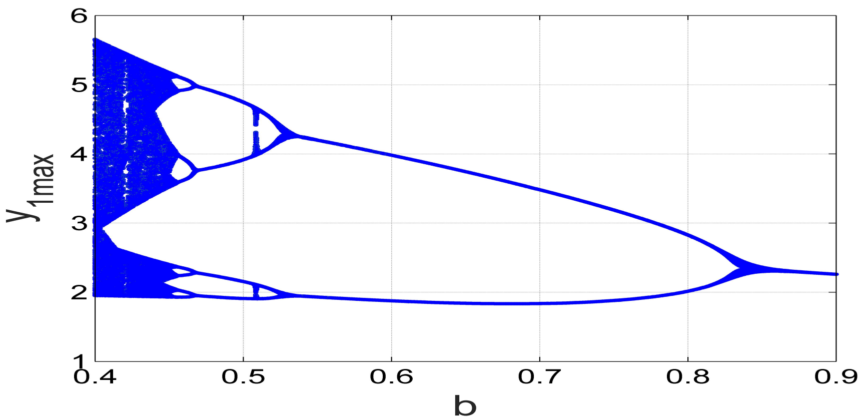

Figure 12: Reversal period doubling cascade in the jerk system (3) when parameter b varies in the interval [0.4, 0.9]

When $b \in ([0.10, 0.44])$, the jerk system (3) has chaotic attractor.

When $b \in ([0.45, 0.47])$, the jerk system (3) has reverse period-8 attractor.

When $b \in ([0.48, 0.53])$, the jerk system (3) has reverse period-4 attractor.

When $b \in ([0.54, 0.85])$, the jerk system (3) has reverse period-2 attractor.

When $b \in ([0.86, 2])$, the jerk system (3) has reverse period-1 attractor, which makes an end for the reverse period-doubling cascade.

The various attractors (numerical simulations) illustrating the above described route to exiting from chaos are listed in Table 2 and plotted in Figure 13.

Table 2: Dynamics, bifurcation diagrams and attractors of the new jerk system (3) with parameter b varying

b range	b value	Dynamics	Bifurcation Diagram	Attractor
$[0.10, 0.45]$	0.4	**Chaos**	Figure 12	Figure 13a
$[0.45, 0.47]$	0.46	Period-8	Figure 12	Figure 13b
$[0.48, 0.53]$	0.49	Period-4	Figure 12	Figure 13c
$[0.54, 0.85]$	0.65	Period-2	Figure 12	Figure 13d
$[0.86, 2]$	1	Period-1	Figure 12	Figure 13e

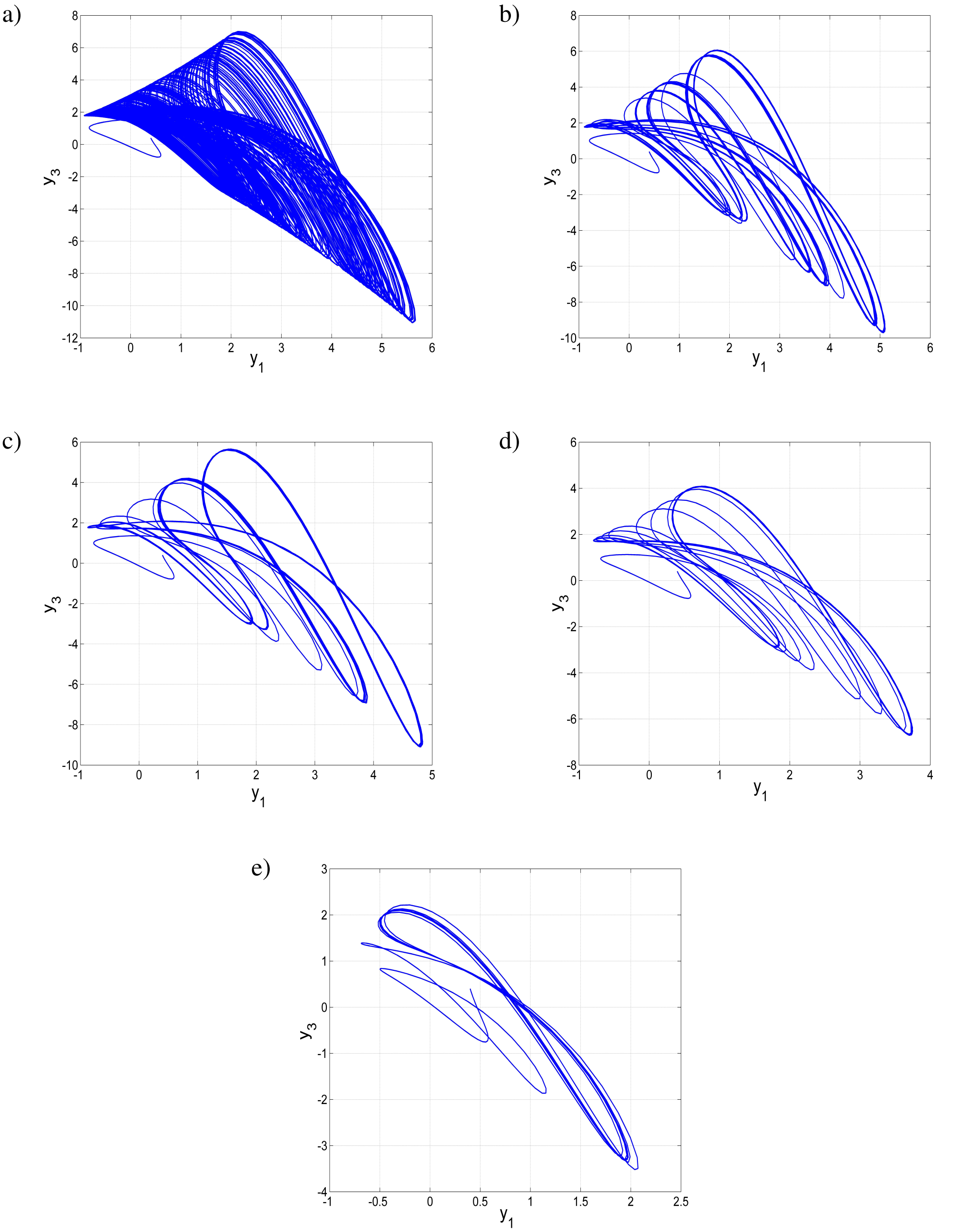

Figure 13: Numerical phase space trajectories showing the classical reverse period doubling in the jerk system (3) when the parameter b varies: a) chaos for$b = 0.4$, b) Reverse period-8 for $b = 0.46$, c) Reverse period-4 for $b = 0.49$, d) Reverse period-2 for $b = 0.65$ and e) Reverse period-1 for $b = 1$

5. Parameter c varying

To investigate the sensitivity of the jerk system (3) to the variation of parameter c value, we fix $a = 2$, $b = 0.1$ and vary c between 0 and 0.6.

Lyapunov exponents spectrum and the corresponding bifurcation diagram of the jerk system (3) when c varies in the interval $[0, 0.6]$ and for the initial state $Y(0) = (0.4, 0.2, 0.4)$ are depicted in Figure 14, where we can see a good agreement between the bifurcation diagram and the Lyapunov exponents spectrum.

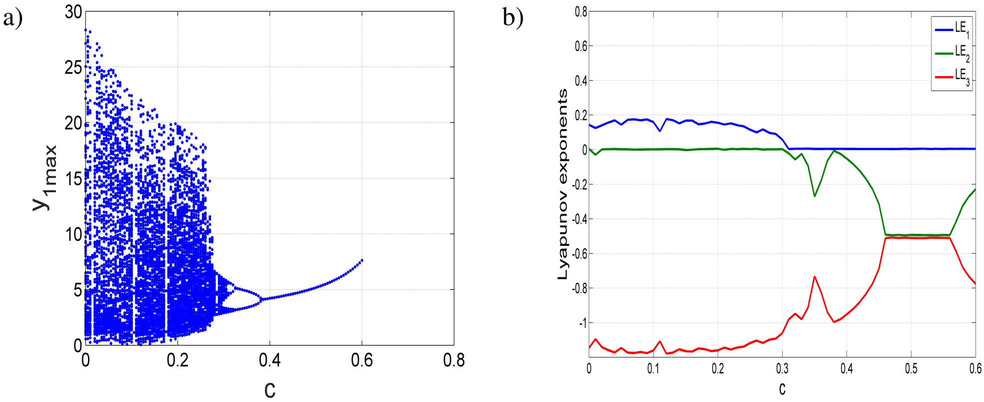

Figure 14: Dynamic analysis of the new jerk system (3) with parameter c varying and $a = 2$, $b = 0.1$: a) Bifurcation diagram and b) Lyapunov exponents spectrum

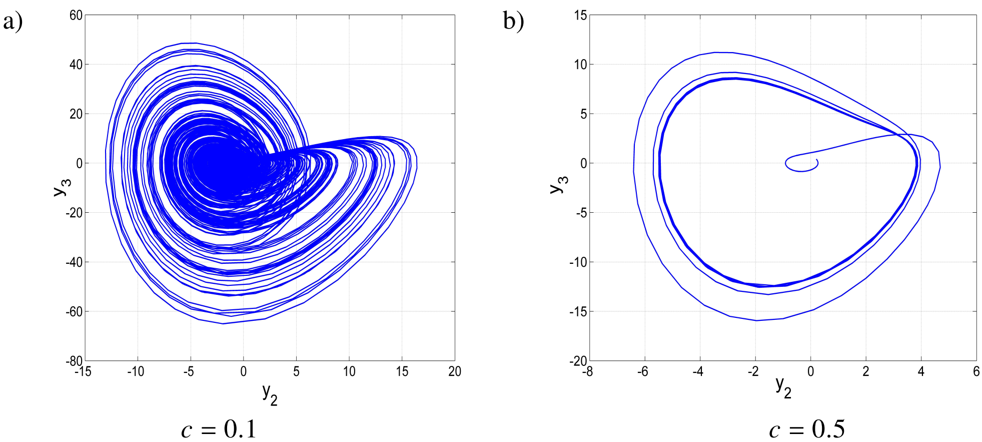

Figure 15: Dynamic analysis of the new jerk system (3) with parameter c varying and $a = 2$, $b = 0.1$: a) Bifurcation diagram and b) Lyapunov exponents spectrum

Figure 14 shows that the proposed jerk system (3) can exhibit chaotic behaviour with one positive Lyapunov exponents when $c \in [0, 0.3]$.

Also, the new system (3) can exhibit periodic behaviour with no positive Lyapunov exponent when $c \in [0.3, 0.6]$, which indicates no complexity of the dynamics. There are also a tiny windows of periodic behaviour sandwiched in chaotic bands when: $c = 0.015$, 0.15 and 0.175.

Different dynamical behaviors of the jerk system (3) for special values of parameter c are shown in Figure 15. In addition, It is clear from the bifurcation diagram of Figure 14 that the jerk system (3) experiences the well-known reversal period-doubling route.

5.1. Reverse period-doubling description

As depicted in the bifurcation diagram of Figure 14 the jerk system (3) experiences period-doubling cascade for increasing values of the parameter c.

Therefore, we can observe the well-known reverse period-doubling exiting from chaos (chaos → period-8 → period-4 → period-2 →period-1) for specified values of parameter c as shown in Figure 16.

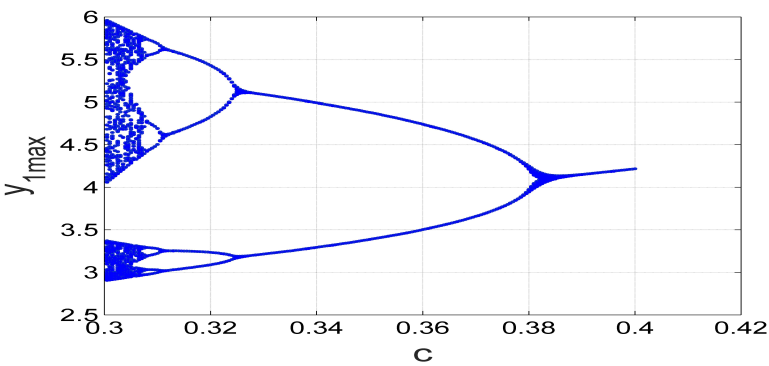

Figure 16: Reversal period doubling cascade in the jerk system (3) when parameter c varies in the interval [0.3, 0.4]

When $c \in [0, 0.3]$, the jerk system (3) has chaotic attractor.

When $c \in [0.30, 0.31]$, the jerk system (3) has reverse period-8 attractor.

When $c \in [0.32, 0.33]$, the jerk system (3) has reverse period-4 attractor.

When $c \in [0.34, 0.38]$, the jerk system (3) has reverse period-2 attractor.

When $c \in [0.39, 0.6]$, the jerk system (3) has reverse period-1 attractor, which makes an end for the reverse period-doubling cascade.

The various attractors (numerical simulations) illustrating the above described route to exiting from chaos are listed in Table 3 and plotted in Figure 17.

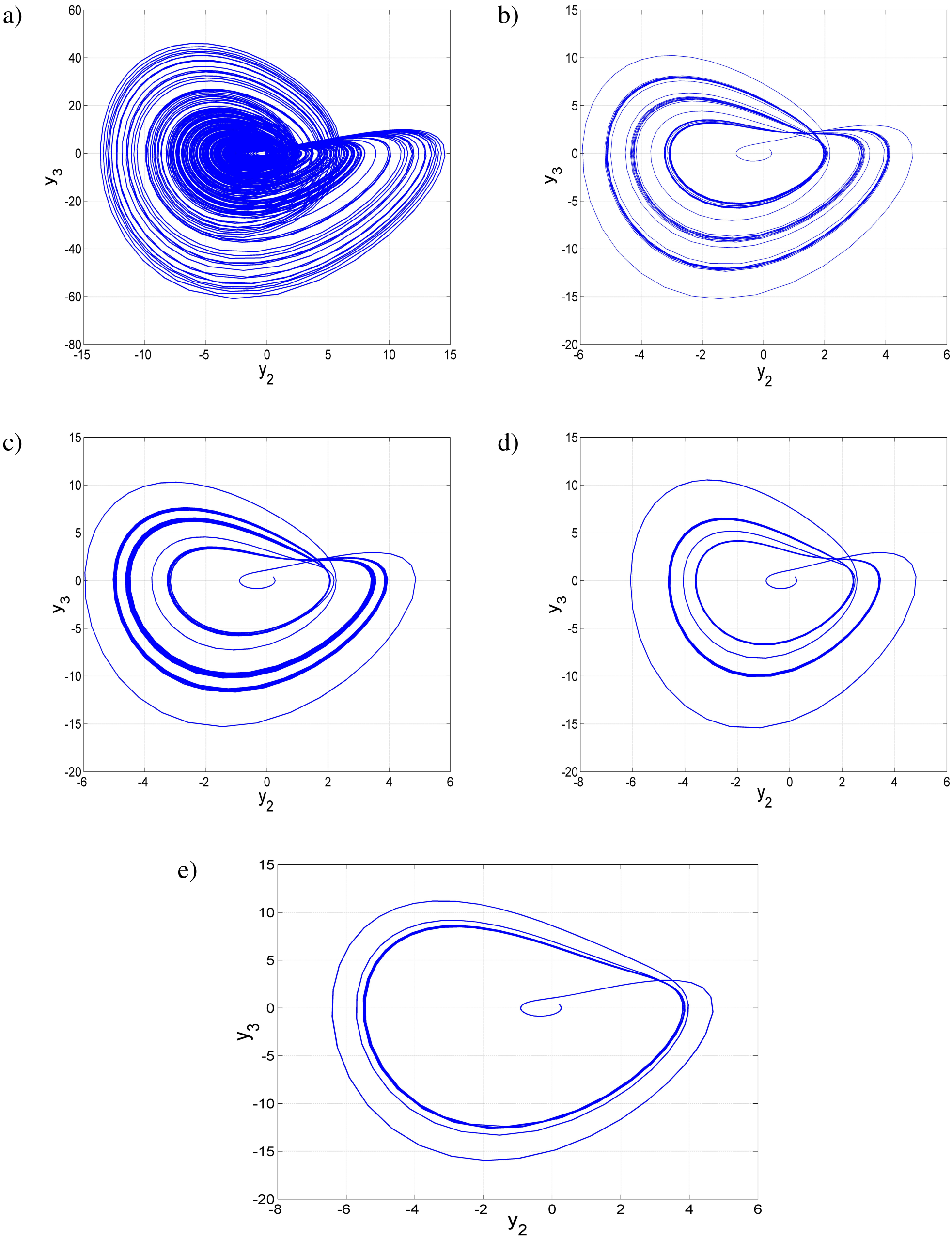

Figure 17: Numerical phase space trajectories showing the classical reverse period doubling in the jerk system (3) when the parameter c varies: a) chaos for$c = 0.2$, b) Reverse period-8 for $c = 0.308$, c) Reverse period-4 for $c = 0.32$, d) Reverse period-2 for $c = 0.36$ and e) Reverse period-1 for $c = 0.5$

Table 3: Dynamics, bifurcation diagrams and attractors of the new jerk system (3) with parameter c varying

c range	c value	Dynamics	Bifurcation Diagram	Attractor
$[0, 0.3]$	0.2	**Chaos**	Figure 14a	Figure 17a
$[0.30, 0.31]$	0.308	Period-8	Figure 16	Figure 17b
$[0.32, 0.33]$	0.32	Period-4	Figure 16	Figure 17c
$[0.34, 0.38]$	0.36	Period-2	Figure 16	Figure 17d
$[0.39, 0.60]$	0.5	Period-1	Figure 16	Figure 17e

6. Backstepping Control Based Synchronization of the New Jerk Systems

As the drive system, we take the new jerk system

$$\begin{aligned}\dot{y}_1 &= y_2\,,\\ \dot{y}_2 &= y_3\,,\\ \dot{y}_3 &= -ay_1 - by_2 - y_3 - y_1y_2 - cy_1^2 + y_2^2\,.\end{aligned}\tag{10}$$

As the response system, we take the new jerk system equipped with a control given by

$$\begin{aligned}\dot{z}_1 &= z_2\,,\\ \dot{z}_2 &= z_3\,,\\ \dot{z}_3 &= -az_1 - bz_2 - z_3 - z_1z_2 - cz_1^2 + z_2^2 + v\,.\end{aligned}\tag{11}$$

We define the synchronization error between the systems (10) and (11) as

$$\begin{aligned}\epsilon_1 &= z_1 - y_1\,,\\ \epsilon_2 &= z_2 - y_2\,,\\ \epsilon_3 &= z_3 - y_3\,.\end{aligned}\tag{12}$$

The error dynamics is calculated as the following:

$$\begin{aligned}\dot{\epsilon}_1 &= \epsilon_2\,,\\ \dot{\epsilon}_2 &= \epsilon_3\,,\\ \dot{\epsilon}_3 &= -a\epsilon_1 - b\epsilon_2 - \epsilon_3 - z_1z_2 + y_1y_2 - c(z_1^2 - y_1^2) + z_2^2 - y_2^2 + v.\end{aligned}\tag{13}$$

First, we define the control v as

$$v = a\epsilon_1 + b\epsilon_2 + \epsilon_3 + z_1z_2 - y_1y_2 + c(z_1^2 - y_1^2) - z_2^2 + y_2^2 + w \tag{14}$$

Substituting (14) into (13), we get the linear control system

$$\dot{\epsilon}_1 = \epsilon_2 \,, \tag{15a}$$
$$\dot{\epsilon}_2 = \epsilon_3 \,, \tag{15b}$$
$$\dot{\epsilon}_3 = w \,. \tag{15c}$$

In (15a), ϵ_2 is regarded as a virtual controller. Thus, we may rewrite (15a) as

$$\dot{\epsilon}_1 = \mu_1 \,, \tag{16}$$

where μ_1 is a control input.

We work with the quadratic positive-definite Lyapunov function

$$P_1(\epsilon_1) = \frac{1}{2}\,\epsilon_1^2 \,. \tag{17}$$

We find that

$$\dot{P}_1 = \epsilon_1\dot{\epsilon}_1 = \epsilon_1\mu_1 \,. \tag{18}$$

We pick the virtual controller as

$$\mu_1 = -\epsilon_1 \,. \tag{19}$$

Then (18) reduces to

$$\dot{P}_1 = -\epsilon_1^2 \tag{20}$$

which is negative definite.

As ϵ_2 and μ_1 start from different initial values, we plan our control design to force ϵ_2 to track the virtual controller μ_1. Hence, the integrator backstepping control is designed to regulate the following output:

$$\xi_1 = \epsilon_2 - \mu_1 = \epsilon_2 + \epsilon_1 \,. \tag{21}$$

We note that

$$\epsilon_2 = \xi_1 - \epsilon_1 \,. \tag{22}$$

Thus, we can write (15a) as

$$\dot{\epsilon}_1 = \xi_1 - \epsilon_1 \,. \tag{23}$$

Furthermore, we observe that

$$\dot{\xi}_1 = \xi_1 - \epsilon_1 + \epsilon_3 \,. \tag{24}$$

In the $(\epsilon_1, \xi_1, \epsilon_3)$ coordinates, the linear control system (15) can be expressed as

$$\dot{\epsilon}_1 = \xi_1 - \epsilon_1 \,, \tag{25a}$$

$$\dot{\xi}_1 = \xi_1 - \epsilon_1 + \epsilon_3\,, \tag{25b}$$
$$\dot{\epsilon}_3 = w\,. \tag{25c}$$

In (25b), ϵ_3 is regarded as a virtual controller. Thus, we may rewrite (25b) as

$$\dot{\xi}_1 = \xi_1 - \epsilon_1 + \mu_2\,, \tag{26}$$

where μ_2 is a control input.

We work with the quadratic positive-definite Lyapunov function

$$P_2(\epsilon_1, \xi_1) = \frac{1}{2}\left(\epsilon_1^2 + \xi_1^2\right). \tag{27}$$

We find that

$$\dot{P}_2 = -\epsilon_1^2 + (\xi_1 + \mu_2)\xi_1\,. \tag{28}$$

We pick the virtual controller as

$$\mu_2 = -2\xi_1\,, \tag{29}$$

Then (28) reduces to

$$\dot{P}_1 = -\epsilon_1^2 - \xi_1^2 \tag{30}$$

which is negative definite.

As ϵ_3 and μ_2 start from different initial values, we plan our control design to force ϵ_3 to track the virtual controller μ_2. Hence, the integrator backstepping control is designed to regulate the following output:

$$\xi_2 = \epsilon_3 - \mu_2 = \epsilon_3 + 2\xi_1\,. \tag{31}$$

We note that

$$\epsilon_3 = \xi_2 - 2\xi_1 = \xi_2 - 2(\epsilon_1 + \epsilon_2). \tag{32}$$

Hence, we have

$$\xi_2 = 2\epsilon_1 + 2\epsilon_2 + \epsilon_3\,. \tag{33}$$

Hence, it follows that

$$\epsilon_3 = \xi_2 - 2\epsilon_1 - 2\epsilon_2\,. \tag{34}$$

Thus, we can write (25b) as

$$\dot{\xi}_1 = -\xi_1 + \xi_2 - \epsilon_1 \tag{35}$$

In the $(\epsilon_1, \xi_1, \xi_2)$ coordinates, the linear system (25) can be represented as

$$\dot{\epsilon}_1 = \xi_1 - \epsilon_1 \tag{36a}$$
$$\dot{\xi}_1 = -\xi_1 + \xi_2 - \epsilon_1 \tag{36b}$$

$$\dot{\xi}_2 = -2\xi_1 + 2\xi_2 - 2\epsilon_1 + w \tag{36c}$$

Finally, we consider the quadratic Lyapunov function

$$P(\epsilon_1, \xi_1, \xi_2) = \frac{1}{2}\left(\epsilon_1^2 + \xi_1^2 + \xi_2^2\right). \tag{37}$$

A simple calculation gives

$$\dot{P} = -\epsilon_1^2 - \xi_1^2 - \xi_2^2 + \xi_2(-\xi_1 + 3\xi_2 - 2\epsilon_1 + w). \tag{38}$$

Thus, we take

$$w = \xi_1 - 3\xi_2 + 2\epsilon_1 - K\xi_2 \qquad (K > 0). \tag{39}$$

Substituting the value of w from (39) into (38), we get

$$\dot{P} = -\epsilon_1^2 - \xi_1^2 - (1 + K)\xi_2^2 \tag{40}$$

which is quadratic and negative definite on $\mathbf{R}^3$.

Hence, by Lyapunov stability theory, the system (15) is globally asymptotically stable.

Simplifying (39), we can write w as

$$w = -3\epsilon_1 - 5\epsilon_2 - 3\epsilon_3 - K\xi_2 \qquad (K > 0). \tag{41}$$

Substituting from (41) into (14) and simplifying, we get the required backstepping control law as

$$\begin{aligned} v = (a - 3)\epsilon_1 + (b - 5)\epsilon_2 - 2\epsilon_3 + z_1 z_2 - y_1 y_2 + c(z_1^2 - y_1^2) \\ - \; z_2^2 + y_2^2 - K\xi_2\,, \end{aligned} \tag{42}$$

where $K > 0$ and $\xi_2 = 2\epsilon_1 + 2\epsilon_2 + \epsilon_3$.

Thus, we have established the following result.

Theorem 1 *The backstepping control law defined by (42) achieves global asymptotic synchronization between the jerk systems (10) and (11) for all initial states* $y(0), z(0) \in \mathbf{R}^3$. □

For MATLAB simulations of the backstepping control system, we take the parameter values of the jerk systems (10) and (11) as in the chaotic case, *viz.* $(a, b, c) = (2, 0.1, 0.2)$. We take the control gain as $K = 20$.

The initial state of the jerk system (10) is taken as

$$y_1(0) = 2.3, \qquad y_2(0) = 5.8, \qquad y_3(0) = 4.9. \tag{43}$$

The initial state of the response system (11) is taken as

$$z_1(0) = 7.6, \qquad z_2(0) = 0.4, \qquad z_3(0) = 2.7. \tag{44}$$

Figure 18 shows that the proposed backstepping control achieves asymptotic synchronization between the chaotic jerk systems (10) and (11).

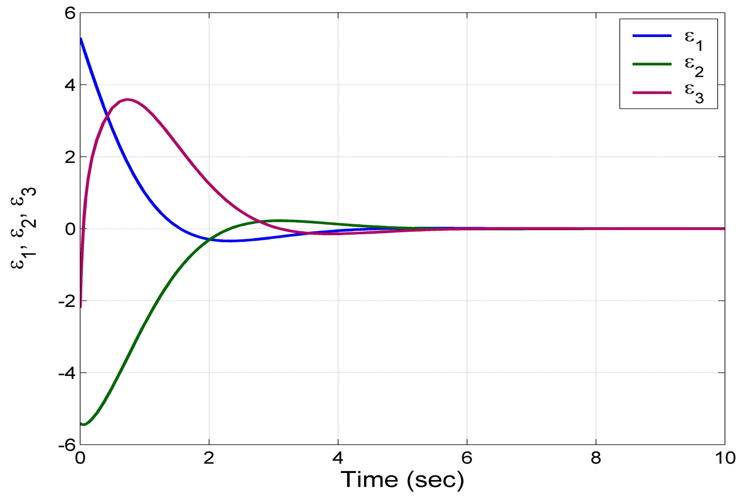

Figure 18: Time-history for the synchronization errors ϵ_1, ϵ_2 and ϵ_3

7. Circuit Simulation of the New Jerk Chaotic System

This section describes the circuit simulation in MultiSim for the new jerk chaotic system (3) proposed in this work. The whole circuit presented in Figure 19 consists of three channels to implement the integration of the three variables y_1, y_2, y_3, respectively. Applying the Kirchhoff laws, the circuit presented in Figure 19 is described by the following equations:

$$\begin{aligned} \dot{y_1} &= \frac{1}{C_1 R_1} y_2 , \\ \dot{y_2} &= \frac{1}{C_2 R_2} y_3 , \\ \dot{y_3} &= -\frac{1}{C_3 R_3} y_1 - \frac{1}{C_3 R_4} y_2 - \frac{1}{C_3 R_5} y_3 \\ &\quad - \frac{1}{10 C_3 R_6} y_1 y_2 - \frac{1}{10 C_3 R_7} y_1^2 + \frac{1}{10 C_3 R_8} y_2^2 . \end{aligned} \tag{45}$$

Here, y_1, y_2, y_3 correspond to the voltages on the integrators U1A, U2A, and U3A, respectively. The values of components in the circuit are selected as: $R_3 = R_7 = 50$ kΩ, $R_6 = R_8 = 10$ kΩ, $R_4 = 1$ MΩ, $R_1 = R_2 = R_5 = R_9 = R_{10} = R_{11} = R_{12} = 100$ kΩ, $C_1 = C_2 = C_3 = 1$ nF. MultiSIM outputs of the circuit (45) are presented in Figure 20. A good qualitative agreement between the MATLAB simulations of the jerk system (3) and circuit implementation is observed.

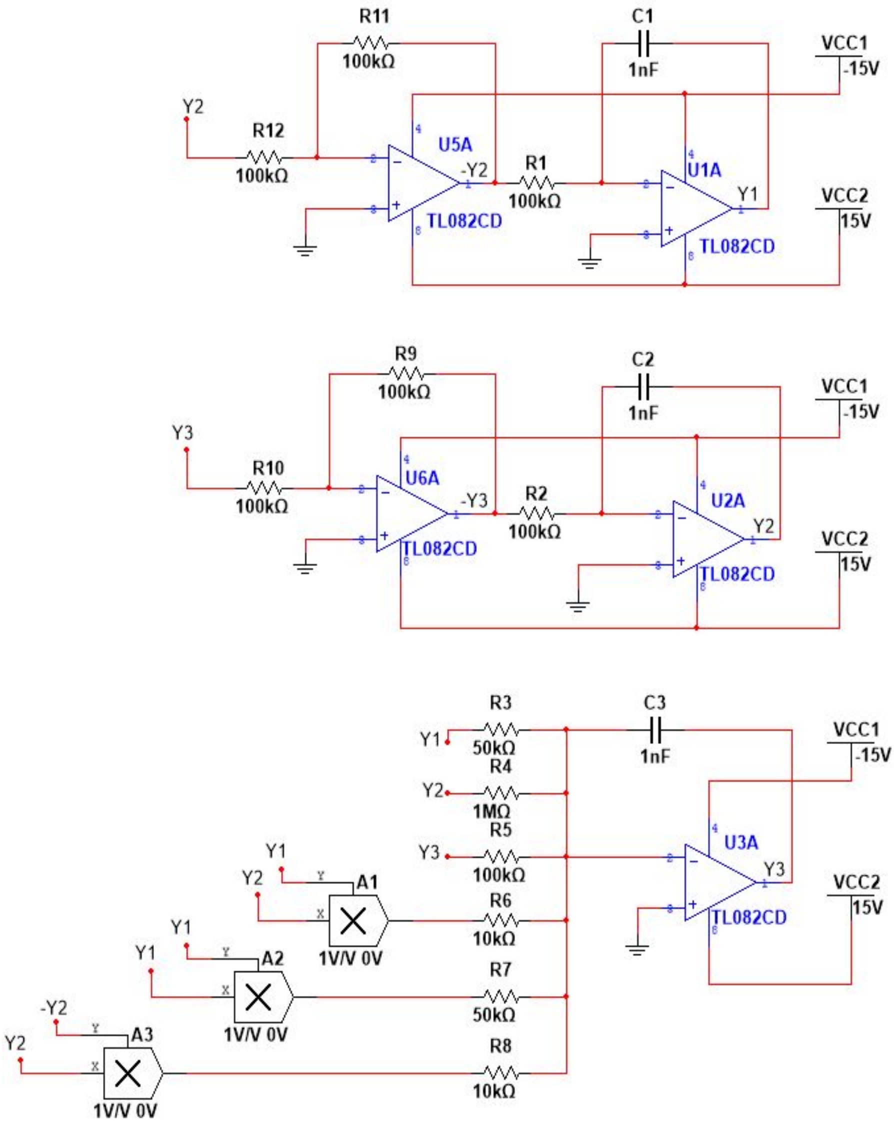

Figure 19: Circuit design of the new chaotic system (45)

Figure 21 demonstrates spectral Fourier analysis for chaotic signals. The frequency range is 5 kHz. For y_1 and y_2 coordinates spectral harmonics are at the level of "–20 dB". For y_3 coordinate spectral harmonics are at the level of "–15 dB". It corresponds to a prevailing frequency of the implementing oscillating loop. The power spectra of the produced signals are broadband, typical of chaotic signals.

a)
b)
c)

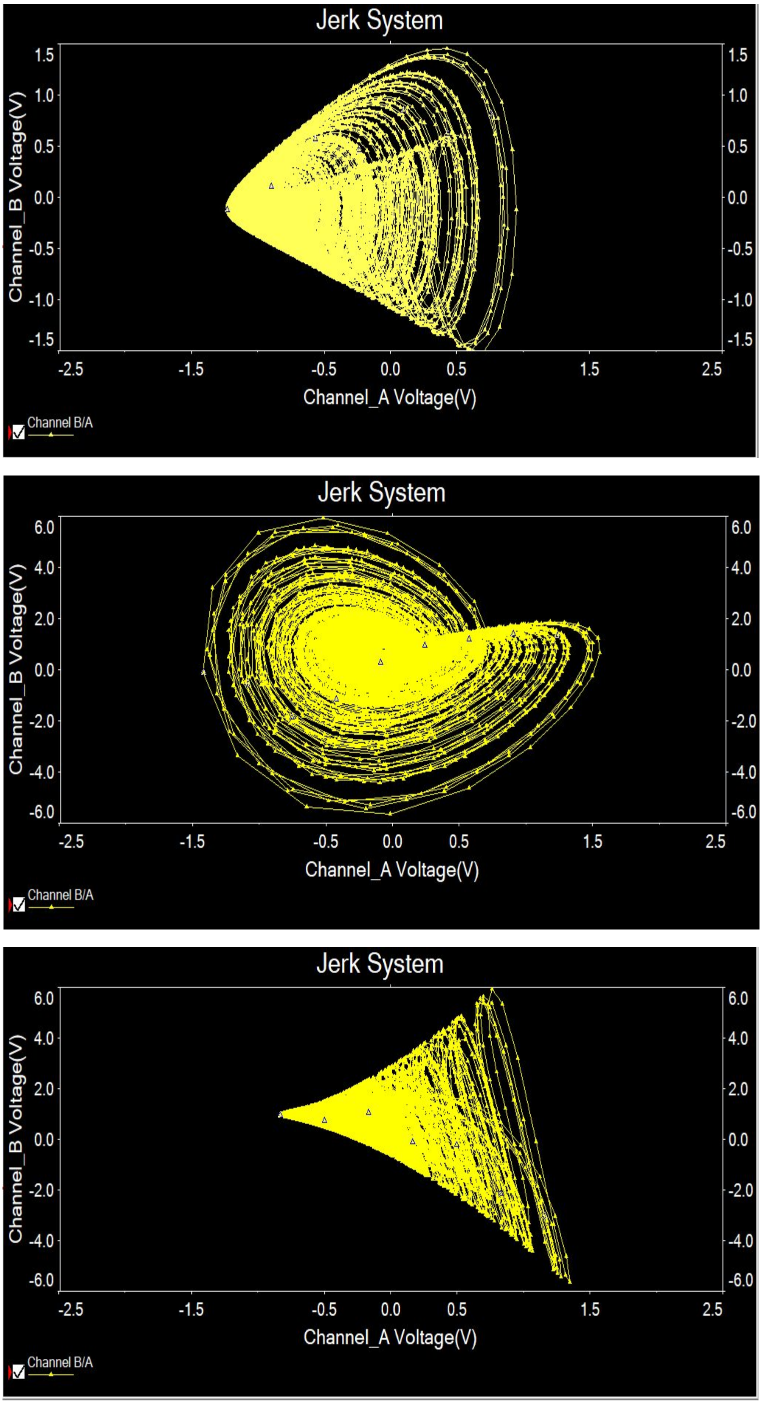

Figure 20: Chaotic attractors of new chaotic system (45) using MultiSim circuit simulation: a) $y_1 - y_2$ plane, b) $y_2 - y_3$ plane and c) $y_1 - y_3$ plane

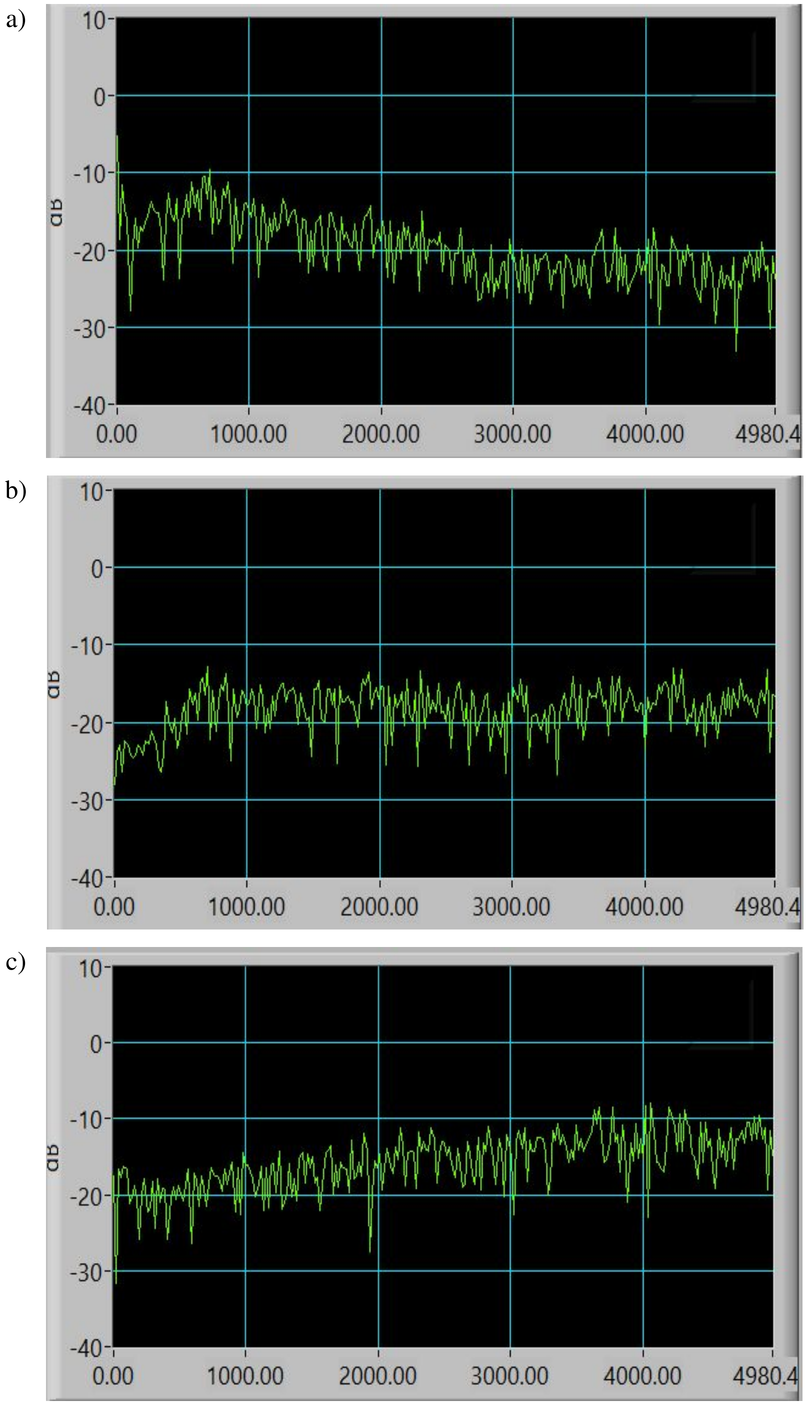

Figure 21: The spectral distribution of new chaotic system (45): a) y_1 signal, b) y_2 signal and c) y_3 signal

8. Conclusions

A new dissipative jerk chaotic system with three quadratic terms was proposed in this research paper. A detailed bifurcation analysis with respect to the variation of the three parameters for the new jerk system was exhibited. We also showed that the proposed system exhibits multistability with coexisting attractors. We also described a backstepping control-based synchronization design for a pair of new jerk chaotic systems. Finally, we used MultiSim to build a circuit simulation model for the new jerk system.

References

[1] O. Spitz, A. Herdt, J. Wu, G. Maisons, M. Carras, C.W. Wong, W. Elsasser, and F. Grillot: Private communication with quantum cascade laser photonic chaos. *Nature Communications*, **12**(1), (2021), Article ID 3327. DOI: 10.1038/s41467-021-23527-9.

[2] X. Mao, Y. Sun, L. Wang, Y. Guo, Z. Gao, Y. Wang, S. Li, L. Yan, and A. Wang: Instability of optical phase synchronization between chaotic semiconductor lasers. *Optics Letters*, **46**(12) (2021), 2824–2827. DOI: 10.1364/OL.413102.

[3] A. Racca and L. Magri: Robust optimization and validation of echo state networks for learning chaotic dynamics. *Neural Networks*, **142** (2021), 252–268. DOI: 10.1016/j.neunet.2021.05.004.

[4] W. Zhu, H. Nikafshan Rad, and M. Hasanipanah: A chaos recurrent ANFIS optimized by PSO to predict ground vibration generated in rock blasting. *Applied Soft Computing*, **108** (2021), Article ID 107434. DOI: 10.1016/j.asoc.2021.107434.

[5] S. Vaidyanathan: Hybrid chaos synchronization of 3-cells cellular neural network attractors via adaptive control method. *International Journal of PharmTech Research*, **8**(8), (2015), 61–73. https://www.sphinxsai.com/2015/ph_vol8_no8/ph01.htm

[6] Z. Yaghoubi and H. Zarabadipour: Hybrid neural-network control of mobile robot system via anti-control of chaos. *Mechatronic Systems and Control*, **48**(4), (2020), 239–248. DOI: 10.2316/J.2020.201-0058.

[7] E. Petavratzis, L. Moysis, C. Volos, I. Stouboulos, H. Nistazakis, and K. Valavanis: A chaotic path planning generator enhanced by a mem-

ory technique. *Robotics and Autonomous Systems*, **143** (2021), Article ID 103826. DOI: 10.1016/j.robot.2021.103826.

[8] Q. Shi, Y. Gao, Z. Li, J. Wan, and R. Shi: High-dynamic-range infrared radiometer based on chaos detection method. *Infrared Physics and Technology*, **116** (2021), Article ID 103787. DOI: 10.1016/j.infrared.2021.103787.

[9] A. Russomanno, M. Fava, and R. Fazio: Chaos and subdiffusion in infinite-range coupled quantum kicked rotors. *Physical Review B*, **103**(22), (2021), Article ID 224301. DOI: 10.1103/PhysRevB.103.224301.

[10] E. Zambrano-Serrano and A. Anzo-Hernandez: A novel antimonotic hyperjerk system: Analysis, synchronization and circuit design. *Physica D: Nonlinear Phenomena*, **424** (2021), Article ID 132927. DOI: 10.1016/j.physd.2021.132927.

[11] K. Tian, C. Grebogi, and H-P. Ren: Chaos generation with impulse control: Application to non-chaotic systems and circuit design. *IEEE Transactions on Circuits and Systems I: Regular Papers*, **68**(7), (2021), 3012–3022. DOI: 10.1109/TCSI.2021.3075550.

[12] J. Ying, Y. Liang, J. Wang, Y. Dong, G. Wang, and M. Gu: A tristable locally-active memristor and its complex dynamics. *Chaos, Solitons and Fractals*, **148** (2021), Article ID 111038. DOI: 10.1016/j.chaos.2021.111038.

[13] Q. Gio, N. Wang, and G. Zhang: A novel current-controlled memristor-based chaotic circuit. *Integration*, **80** (2021), 20–28. DOI: 10.1016/j.vlsi.2021.05.008.

[14] S. Vaidyanathan and C. Volos: *Advances in Memristors, Memristive Devices and Systems*. Springer, Berlin, Germany, 2017.

[15] P. Sarasu and V. Sundarapandian: Adaptive controller design for the generalized projective synchronization of 4-scroll systems. *International Journal of Systems Signal Control and Engineering Application*, **5**(2), (2012), 21–30. DOI: 10.3923/ijssceapp.2012.21.30.

[16] S. Vaidyanathan: Output regulation of Arneodo-Coullet chaotic system. *Communications in Computer and Information Science*, **133** (2011), 98–107. DOI: 10.1007/978-3-642-17881-8_10.

[17] F.S. Hasan: Design and analysis of grouping subcarrier index modulation for differential chaos shift keying communication system. *Physical Communication*, **47** (2021), Article ID 101325. DOI: 10.1016/j.phycom.2021.101325.

[18] P. Zanardi and N. Anand: Information scrambling and chaos in open quantum systems. *Physical Review A*, **103**(6) (2021), Article ID 062214. DOI: 10.1103/PhysRevA.103.062214.

[19] A. Sambas, S. Vaidyanathan, I.M. Moroz, B. Idowu, M.A. Mohamed, M. Mamat, and W.S.M. Sanjaya: A simple multi-stable chaotic jerk system with two saddle-foci equilibrium points: Analysis, synchronization via backstepping technique and MultiSim circuit design. *International Journal of Electrical and Computer Engineering*, **11**(4) (2021), 2941–2952. DOI: 10.11591/ijece.v11i4.pp2941-2952.

[20] C. Li, J.C. Sprott, W. Joo-Chen Thio, and Z. Gu: A simple memristive jerk system. *IET Circuits, Devices and Systems*, **15**(4), (2021), 388–382. DOI: 10.1049/cds2.12035.

[21] F. Braun and A.C. Mereu: Zero-Hopf bifurcation in a 3D jerk system. *Nonlinear Analysis: Real World Applications*, **59** (2021), Article ID 103245. DOI: 10.1016/j.nonrwa.2020.103245.

[22] L. Kamdjeu Kengne, Y.P. Kamdeu Nkandeu, J.R. Mboupda Pone, A. Tiedeu, and H.B. Fotsin: Image encryption using a novel quintic jerk circuit with adjustable symmetry. *International Journal of Circuit Theory and Applications*, **49**(5) (2021), 1470–1501. DOI: 10.1002/cta.2968.

[23] Q. Xu, S. Cheng, Z. Ju, M. Chen, and H. Wu: Asymmetric coexisting bifurcations and multi-stability in an asymmetric memristive diode-bridge-based Jerk circuit. *Chinese Journal of Physics*, **70** (2021), 69–81. DOI: 10.1016/j.cjph.2020.11.007.

[24] K. Lamamra, S. Vaidyanathan, W.T. Putra, E. Darnila, A. Sambas, and Mujiarto: A new 3-D chaotic jerk system with four nonlinear terms, its backstepping synchronization and circuit simulation. *Journal of Physics: Conference Series*, **1477**(2) (2020), Article ID 022017. DOI: 10.1088/1742-6596/1477/2/022017.